Supplemental Information

Design of External Fluid Handling Components

A number of external fluid handling components were added to the device to address experimental needs (Supplemental Figure 1). These components addressed requirements associated with device priming, device loading, maintaining sterility, and performing microscopy on live samples. Importantly, all fluid handling components could be sterilized by autoclaving, by ethylene oxide treatment, or were purchased sterile.

The device inlet was chosen to satisfy requirements associated with priming, loading aggregates, and culture. In order to prime devices to remove bubbles prior to loading, devices were pressurized with fluid using a syringe screwed onto the luer lock connection of the inlet (Supplemental Figure 1). For loading of aggregates and subsequent culture, a standard 3 mL syringe with the plunger removed was screwed on to the device inlet as a media reservoir. This provided a volume large enough that that the reservoir needed to be filled only once per day or less.

Two types of valves were used. The pinch valve was used during priming to maintain pressurization of the device. During aggregate loading and in all following device manipulations, the two-way valve was used to stop flow through the device as opposed to the pinch valve. The pinch valve displaced fluid back into the device that could dislodge trapped aggregates, whereas the two-way valve displaced a minimal amount of fluid.

To perfuse media at a defined rate and frequency during culture, the outlet tubing was connected to a syringe on a syringe pump. The pump was programmed to withdraw media from the media reservoir, through the device, at defined rate and frequency.

Finally, during experiments, devices containing live aggregates needed to be transported sterilely between biosafety cabinets, incubators, and microscopes. The syringe filter at the device outlet provided a sterile barrier, and sterile, gas-permeable adhesive film was used to create a sterile barrier at the opening to the media reservoir. For live microscopy, the media reservoir could be unscrewed from the device inlet and the device inlet sterilely sealed with a luer lock connector in order to fit on a confocal or epifluorescent microscope.

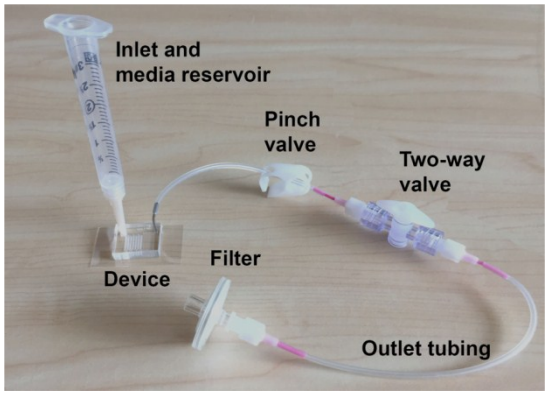

Supplemental Figure 1. Device and external fluid handling components. Photograph depicts the microfluidic device and external components, including the inlet and media reservoir, valves, outlet tubing, and filter.

Transport modeling

Supplemental Table 1: Transport modeling parameters

Parameter Name	Symbol	Value
Diffusion coefficient, glucose [ref 1]	$D_{glucose}$	$6 \times 10^{-10}\ m^2\ s^{-1}$
Diffusion coefficient, growth factor [ref 1]	$D_{growth\ factor}$	$2 \times 10^{-11}\ m^2\ s^{-1}$
Viscosity, water	μ_{water}	$8.9 \times 10^{-3}\ dyn\ s\ cm^{-2}$
Consumption rate, glucose [ref 1]	$K_{glucose}$	$1 \times 10^{-17}\ mol\ cell^{-1} s^{-1}$
Consumption rate, growth factor[ref 2]	$K_{growth\ factor}$	$2 \times 10^{-22}\ mol\ cell^{-1} s^{-1}$
Initial concentration, glucose	$C_{initial,\ glucose}$	$25\ mol\ m^{-3}$
Trap depth	$L_{trap,\ depth}$	$550\ \mu m$
Trap height	$L_{trap,height}$	$400\ \mu m$
Channel width and height	$h_{channel}$	$300\ \mu m$
Total channel length	$L_{channel}$	80 mm
Volume of trap	V_{trap}	$0.06\ \mu L$
Volume of device	V_{device}	$20\ \mu L$
Number of cells per aggregate [ref 3]	N_{cells}	4000
Number of aggregates per device	$N_{aggregates}$	70
Average linear velocity, continuous perfusion	v_c	$30\ \mu m\ s^{-1}$
Average linear velocity, discontinuous perfusion	v_d	$600\ \mu m\ s^{-1}$

For continuous perfusion, we calculated the time scale, τ_{rxn}, for glucose to be completely consumed by all aggregates in the device. We defined $\tau_{rxn} = (C_{initial} V_{device})/(K_{glucose} N_{aggregates} N_{cells})$ where $C_{initial}$ is the initial glucose concentration, V_{device} is the device volume, $K_{glucose}$ is the cell consumption rate of glucose, $N_{aggregates}$ is the number of aggregates, and N_{cells} is the number of cells per aggregate[3]. Values for these parameters are listed in Supplemental Table 1.

We found that $\tau_{rxn} \approx$ 50 hours. This time scale for glucose consumption was compared to the convective time scale in the main channel, $\tau_{conv} = L_{device}/v_c$ where L_{device} is the linear length through the main serpentine channel of the device and v_c is average linear velocity for continuous perfusion. This convective time scale represents the residence time of a fluid element flowing through the main channel of the device. We found that $\tau_{conv} \approx$ 0.75 hours.

These calculations indicate that the time scale of convection is much faster than that of glucose consumption. This assumes a constant velocity through the device, whereas the velocity actually varies. For v_c one order of magnitude lower, that $\tau_{conv} \approx$ 7.5 hours, which is still << τ_{rxn}.

To assess whether the time interval between media exchanges was sufficient for discontinuous perfusion, we again calculated the time scale, τ_{rxn}, for glucose to be completely consumed in the device. This value was the same as for continuous perfusion: $\tau_{rxn} \approx 50\ hours$, indicating that exchanging media at least once per day was likely sufficient.

As fluid shear stress can modulate cell behavior, we calculated the shear stress for all perfusion conditions tested. Shear stress is defined as $T = (6\mu Q)/(h^2 w)$ where T is fluid shear stress, μ is viscosity of water, Q is the volumetric flow rate, h is the main channel height, and w is the main channel width. For the range of device operating conditions, shear stress was within $T \approx 0.005 - 0.01\ dyn\ cm^{-2}$. As operation at shear stresses $\ll 1\ dyn\ cm^{-2}$ is considered not likely to affect cell phenotype[4], we assumed shear did not have a significant effect in our system.

To assess whether continuous perfusion can remove cell-secreted factors, we calculated the Peclet number, Pe, which represents the ratio between convection and diffusion. We defined $Pe = (L_{trap,\,depth} v_c)/D_{growth\ factor}$ where $L_{trap,\,depth}$ is the trap depth, v_c is the average linear fluid velocity, and $D_{growth\ factor}$ is the diffusion coefficient of a growth factor. For continuous perfusion, we calculated $Pe \approx 850 \gg 1$ for transport of a cell-secreted molecule such as a growth factor, indicating that convection dominates and can indeed perturb cell-secreted signaling.

Correlations between Olig2 expression and other parameters

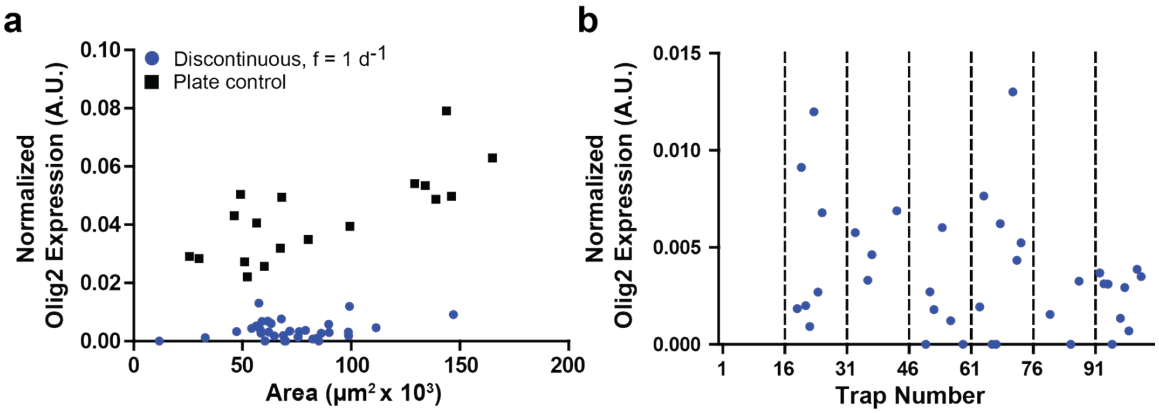

Supplemental Figure 2. Effects of aggregate size and device position on pMN differentiation. a) Correlation between aggregate area and normalized Olig2 expression at day 7. b) Normalized Olig2 expression for aggregates in a single representative device plotted based on position in the device. Traps are numbered with respect to position along the serpentine channel, with trap 1 at the inlet and trap 105 at the outlet.

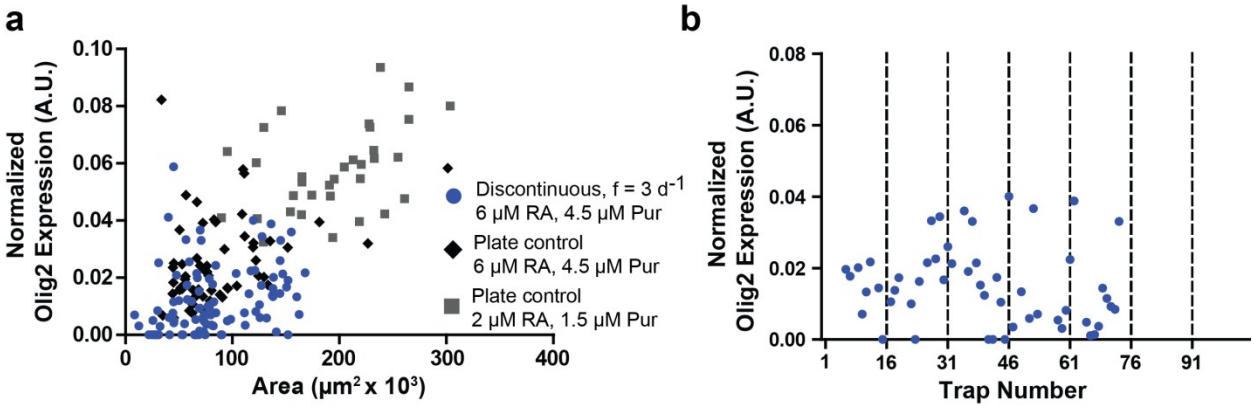

Supplemental Figure 3. Effects of aggregate size and device position on pMN differentiation. a) Relationship between aggregate area and normalized Olig2 expression at day 7. b) Normalized Olig2 expression for aggregates in a single representative device plotted based on position in the device. Traps are numbered with respect to position along the serpentine channel, with trap 1 at the inlet and trap 105 at the outlet.

Differentiation of MNs and OPCs

As it is known that during differentiation pMNs generate both MNs and OPCs, we investigated whether these cell types were generated in the $f = 3\ d^{-1}$ microfluidic cultures. To assess generation of MNs, we performed immunostaining for the MN marker Hb9. Hb9 expression was observed both in microfluidic cultures and in plate controls, as seen in the representative images (Supplemental Figure 4a). Quantification of Hb9 expression using image analysis showed culture format and concentration dependent effects (Supplemental Figure 4b). Microfluidic cultures ($f = 3\ d^{-1}$; 6 μM RA, 4.5 μM Pur) on average expressed Hb9 at low levels, with some variability in amount of expression. Plate controls at the same supplemented concentration of small molecules (6 μM RA, 4.5 μM Pur) had slightly higher levels of Hb9 expression ($p<0.0001$). Plate controls at lower small molecule concentrations (2 μM RA, 1.5 μM Pur) had the highest levels of Hb9 expression ($p<0.001$).

In the same experiment, we assessed generation of OPCs by performing immunostaining for Nkx2.2. As depicted in the representative images (Supplemental Figure 4c) and confirmed by quantification (Supplemental Figure 4d), Nkx2.2 expression was observed at low levels in microfluidic cultures and plate controls at the same supplemented RA and Pur concentration. Nkx2.2 expression was much higher in plate controls at the higher RA and Pur concentrations ($p<0.0001$ versus microfluidic culture; $p<0.01$ versus plate controls at the higher concentration).

Together, this data demonstrates that pMNs give rise to both committed MNs and OPCs in these cultures. In the microfluidic cultures, amounts of both cell types are lower than in plate controls, and in particular, microfluidic cultures show very little differentiation of Nkx2.2+ OPCs.

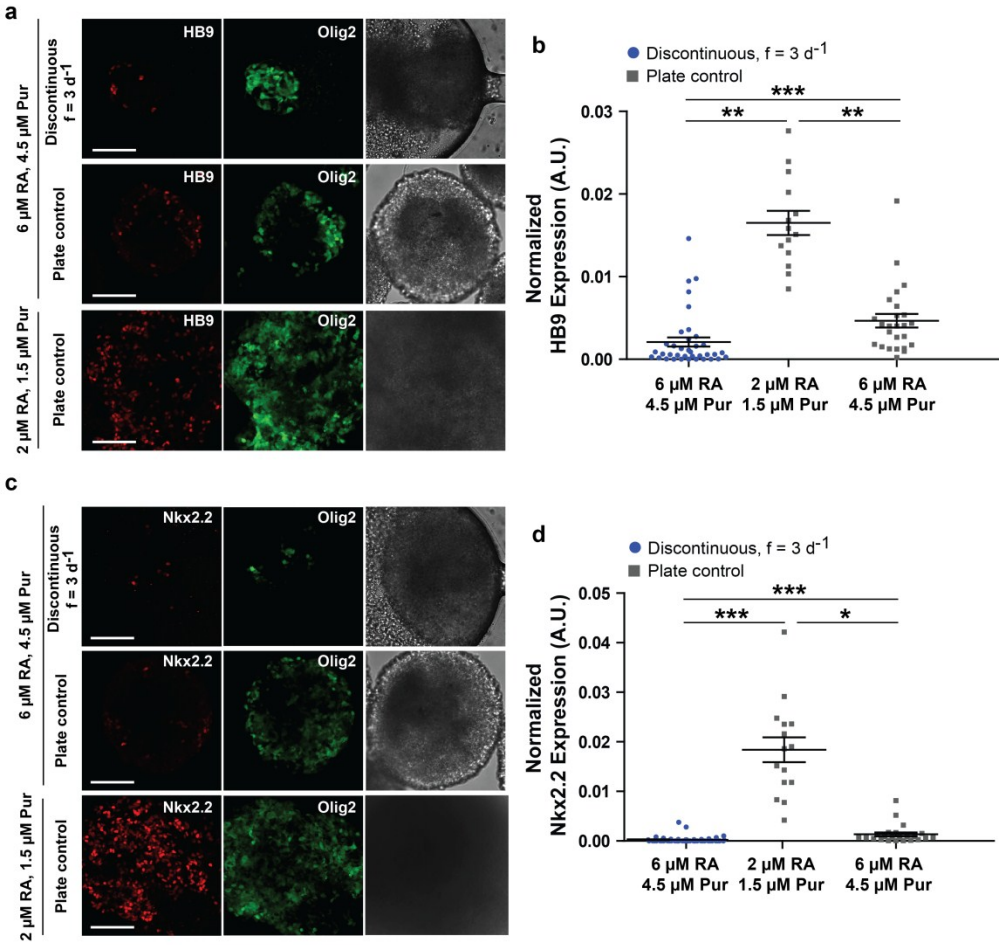

Supplemental Figure 4. Effects of discontinuous perfusion and RA and Pur concentration on expression of Hb9 and Nkx2.2. a) Representative images from a single confocal slice of normalized Hb9 and Olig2 expression at day 7 and corresponding transmitted light images. All scale bars are 100 μm. b) Normalized Hb9 expression quantified for each condition. Discontinuous device: n = 37 from 1 device. Plate control (6 μM/4.5 μM): n = 25. Plate control (2 μM/1.5 μM): n = 14. Error bars represent SEM. Kruskal-Wallis test with Dunns multiple comparisons was used. ** indicates $p < 0.001$; *** indicates $p < 0.0001$. c) Representative images from a single confocal slice of normalized Nkx2.2 and Olig2 expression at day 7 and corresponding bright field images. All scale bars are 100 μm. d) Normalized Nkx2.2 expression quantified for each condition. Discontinuous device: n = 56 from 1 device. Plate control (6 μM/4.5 μM): n = 23. Plate control (2 μM/1.5 μM): n = 15. Error bars represent SEM. Kruskal-Wallis test with Dunns multiple comparisons was used. * indicates $p < 0.01$; *** indicates $p < 0.0001$.

Influence of Device Asymmetry on Microenvironment and pMN Differentiation

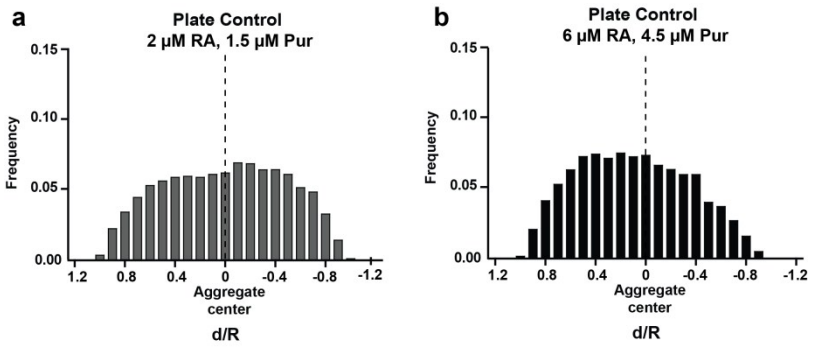

Supplemental Figure 5. Histograms show population-level data for horizontal position of Olig2+ cells with respect to aggregate center line. The orientation of the center line was arbitrarily chosen to be vertical in the confocal images (as opposed to device aggregates, in which the orientation is meaningful).

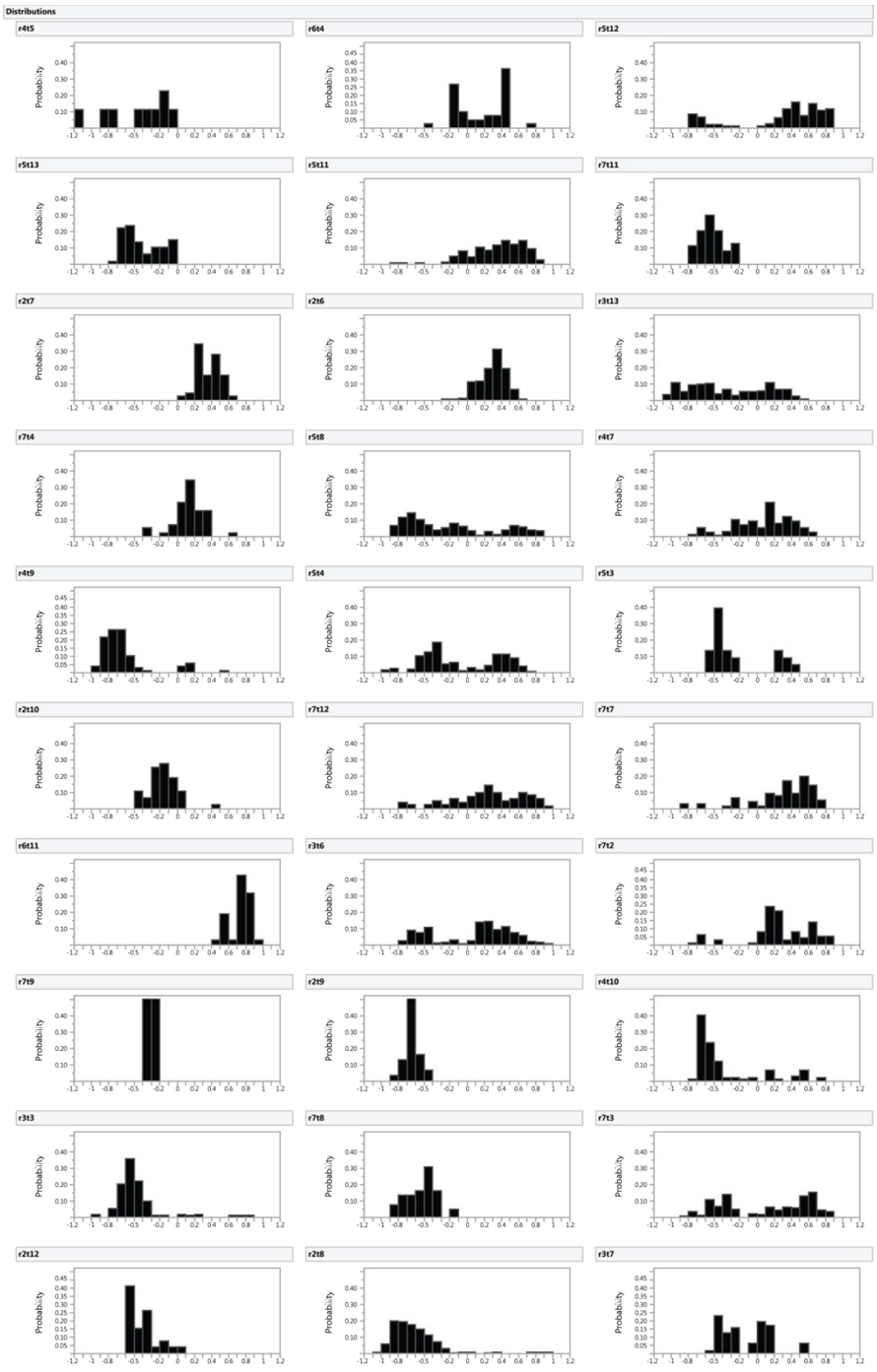

Supplemental Figure 6. Histograms show horizontal position of Olig2+ cells with respect to aggregate center line for discontinuous perfusion (f = 1 d^{-1}) with 2 µM RA and 1.5 µM Pur. Zero indicates aggregate center line, positive numbers indicate portion of aggregate closer to trap entrance, and negative numbers indicate portion of aggregate closer to back of trap.

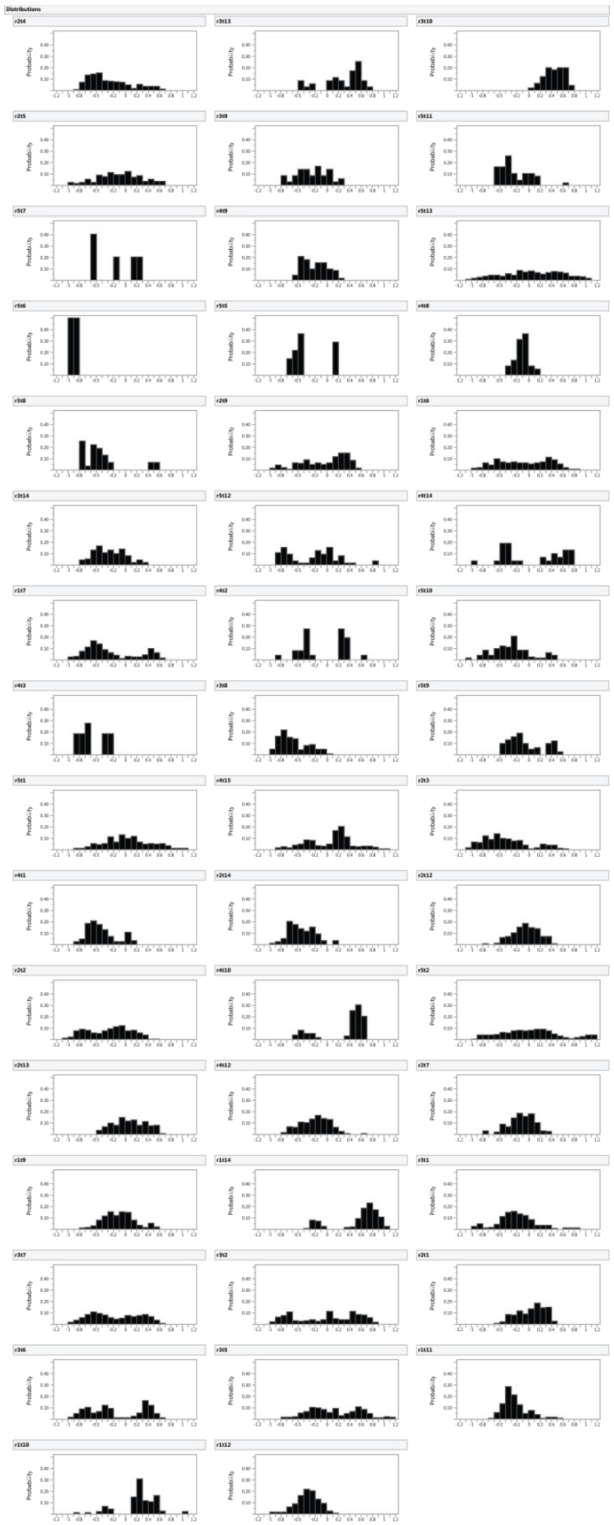

Supplemental Figure 7. Histograms show horizontal position of Olig2+ cells with respect to aggregate center line for discontinuous perfusion (f = 3 d^{-1}) with 6 µM RA and 4.5 µM Pur, one device. Zero indicates aggregate center line, positive numbers indicate portion of aggregate closer to trap entrance, and negative numbers indicate portion of aggregate closer to back of trap.

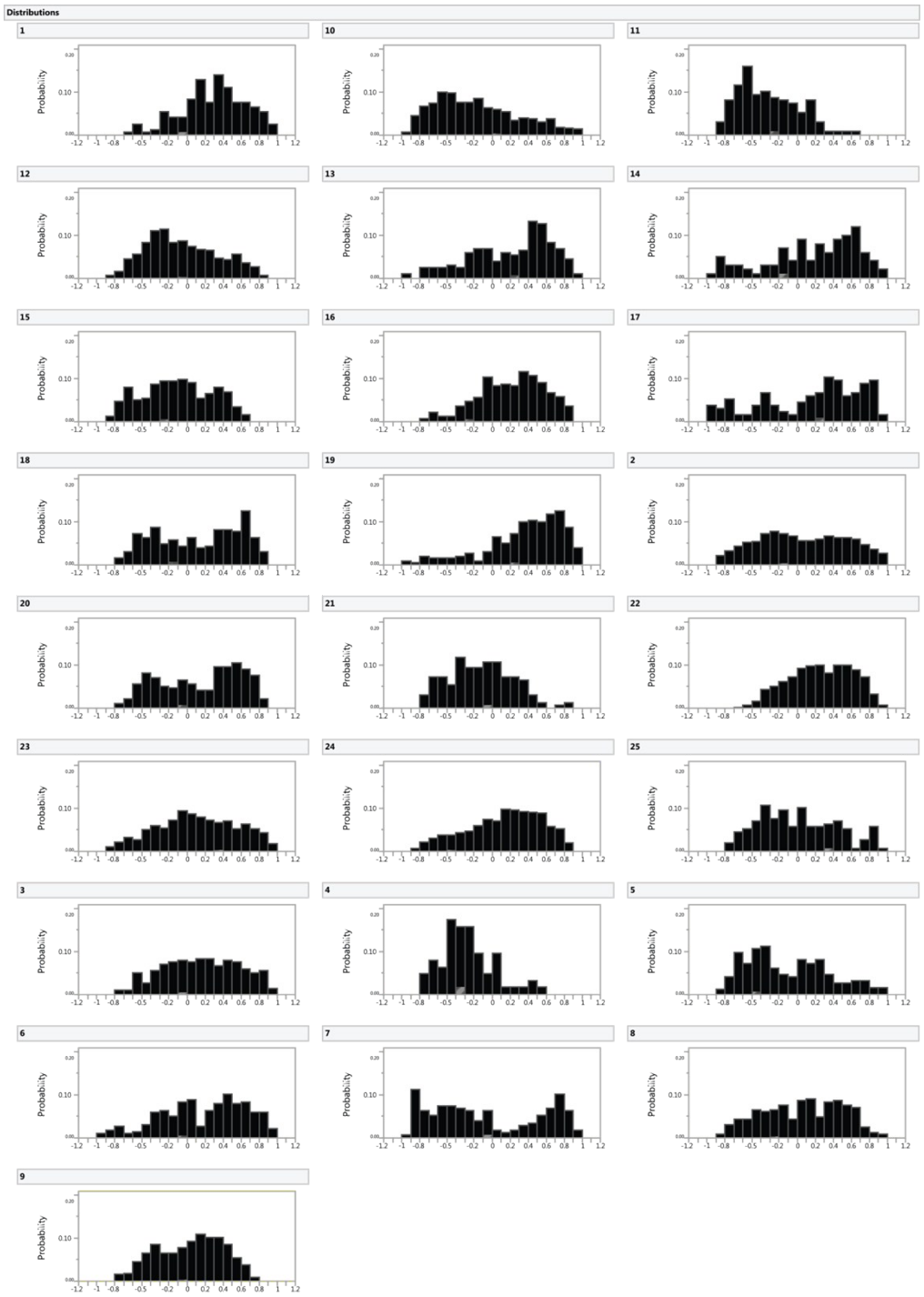

Supplemental Figure 8. Histograms show horizontal position of Olig2+ cells with respect to aggregate center line for plate controls with 6 µM RA and 4.5 µM Pur. Zero indicates aggregate center line, positive numbers indicate portion of aggregate closer to trap entrance, and negative numbers indicate portion of aggregate closer to back of trap.

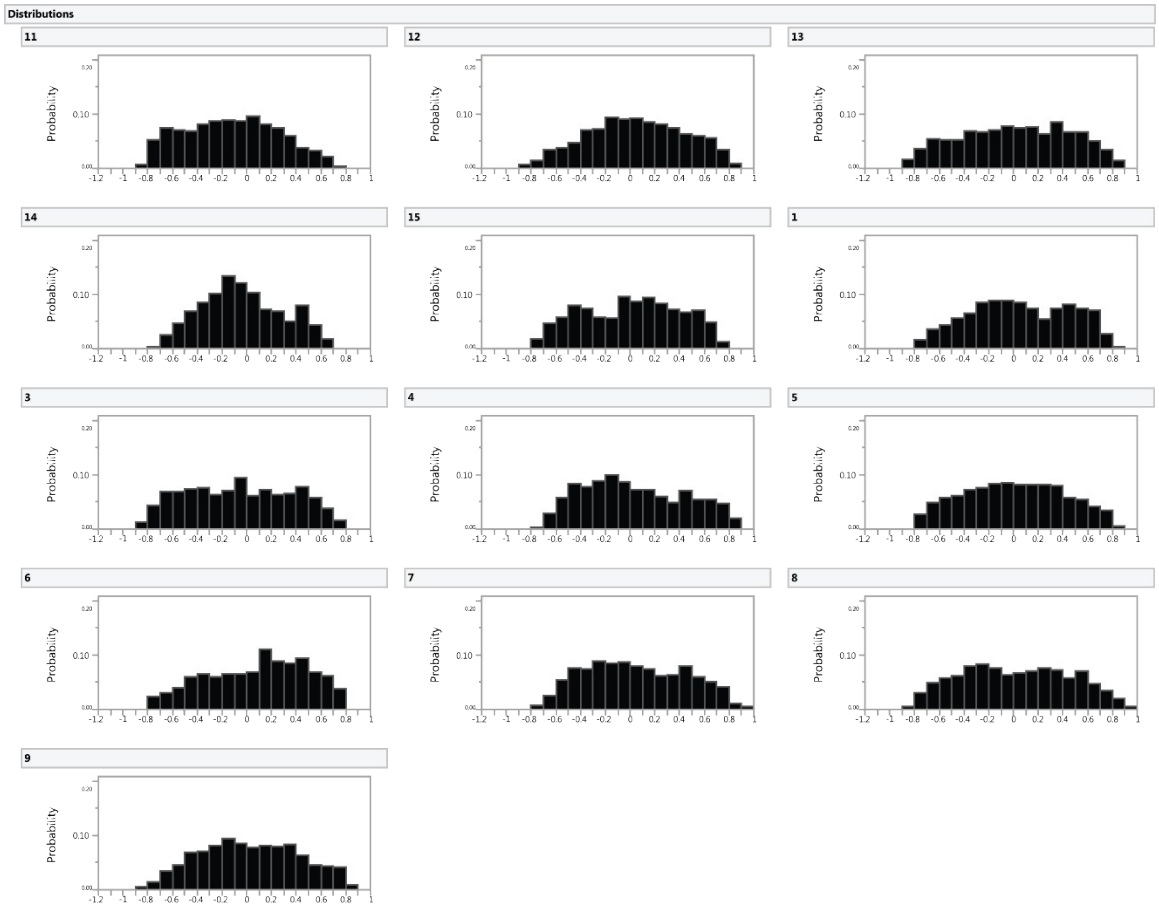

Supplemental Figure 9. Histograms show horizontal position of Olig2+ cells with respect to aggregate center line for plate controls with 2 µM RA and 1.5 µM Pur. Zero indicates aggregate center line, positive numbers indicate portion of aggregate closer to trap entrance, and negative numbers indicate portion of aggregate closer to back of trap.

Transport simulations of nutrients, exogenous, and endogenous factors.

COMSOL computational fluid dynamic (CFD) software was used to model mass transport of a representative nutrient, exogenous small molecule, and endogenous cell-secreted growth factor in a single chamber of the device. In all simulations, the 2D steady state model for diffusive mass transport and reaction of a dilute species was solved. We modeled mass transport under no fluid flow in order to model what happens between media exchanges in the device (when there is no flow). We performed a time-dependent study over the time frame of 0 to 24 hours with a step size of one hour. The geometry modeled was that of a single trap of the device with an aggregate located at back of trap with a diameter of 280 µm (an average size, from our experimental data). Fluid properties were assumed to be those of water. A no flux boundary condition was assumed at all walls. Cell consumption/production of each species were modeled as a reaction within the aggregate. To estimate the cell density within an

aggregate, we used a value reported previously for aggregates formed from mESCs of 2.7 x 10^{14} cells/m^3 [3]. The total number of cells per aggregate were calculated based on this cell density and the average aggregate size (~0.36mm for the f = 3 d^{-1} condition). Values used for transport and reaction of each species are listed in Supplemental Table 2 and in Supplemental Figures 10 and 11. These were obtained from literature or estimated. For the exogenous small molecule, we assumed the diffusion coefficient and concentrations to be that of RA. For the cell-secreted growth factor, we used the diffusion coefficient of EGF. Production rates of cell-secreted factors are not well described in literature, so we assessed a range of production/consumption rates based on the consumption rate of EGF from literature. To account for hindered diffusion of species within the aggregate, we did a parameter sweep, with diffusion in the aggregate modeled as equal to, 0.5x, or 0.1x the diffusion coefficient in water.

Supplemental Table 2: Values for transport and reaction of each species.

Species	**Diffusion Coefficient (m^2 s^{-1})**	**Initial Concentration (mol m^{-3})**	**Boundary Condition Concentration (mol m^{-3})**	**Consumption/ Production Rate (mol $cell^{-1}$ s^{-1})**
Glucose	6×10^{-10}	25	25	1×10^{-17} [ref 1]
Exogenous small molecule	3.8×10^{-10}	6×10^{-3}	6×10^{-3}	2×10^{-22} [ref 2]
Cell-secreted growth factor	2×10^{-11}	0	0	1×10^{-21} [estimated]

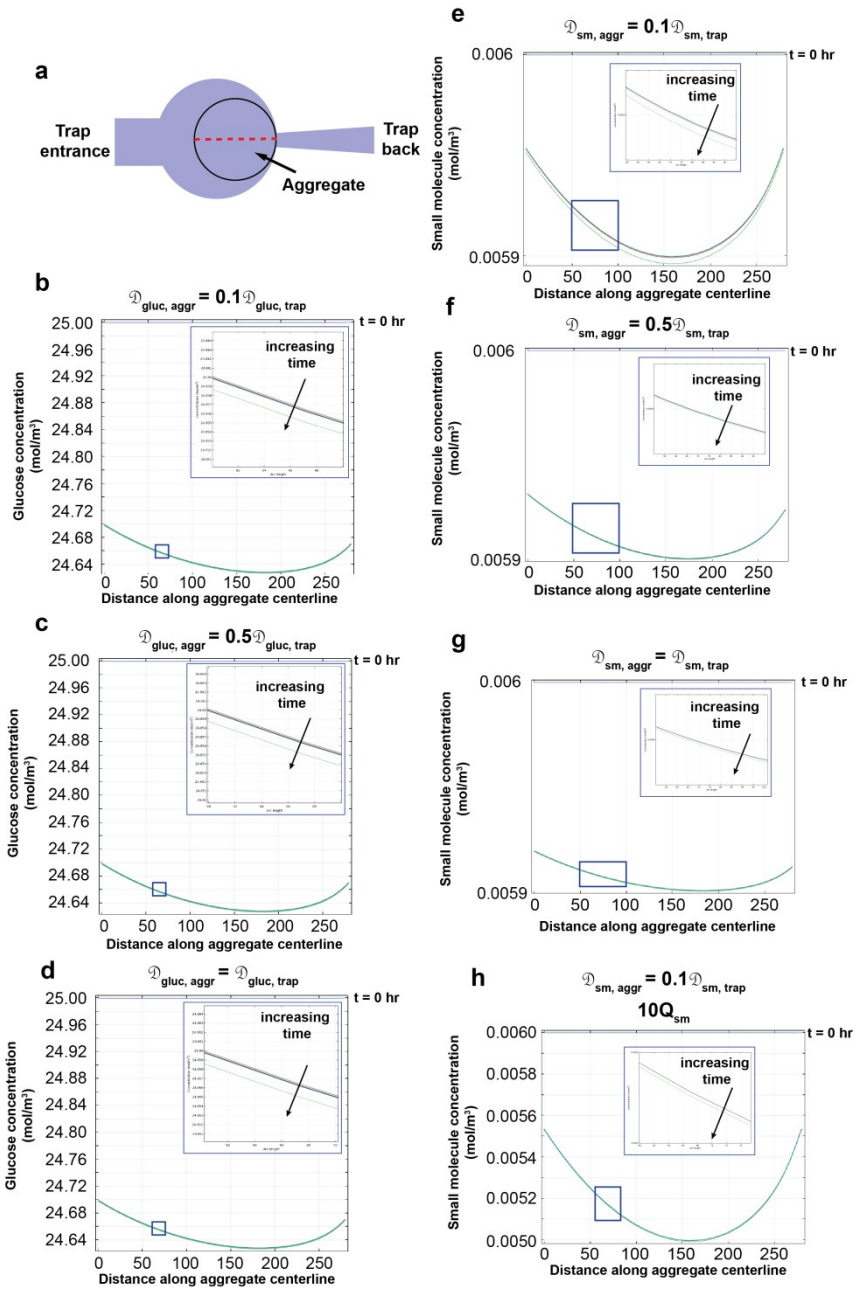

Supplemental Figure 10. Modeling consumption of glucose and an exogenously delivered small molecule. a) Geometry modeled. b-d) Concentration of glucose along the horizontal centerline of the aggregate (as depicted in red in a) for 0-24 hours for three different values of the glucose diffusion coefficient in the aggregate ($D_{gluc,aggr}$). Insets show a zoomed in version of indicated part of plot. f-h) Concentration of a small molecule along the horizontal centerline of the aggregate (as depicted in red in a) for 0-24 hours for three different values of the diffusion coefficient in the aggregate ($D_{sm,aggr}$)and two different consumption rates (Q_{sm}). Insets show a zoomed in version of indicated part of plot. Each line represents a time point from 0 to 24 hours, with a step of 1 hour. Time increases in the direction indicated.

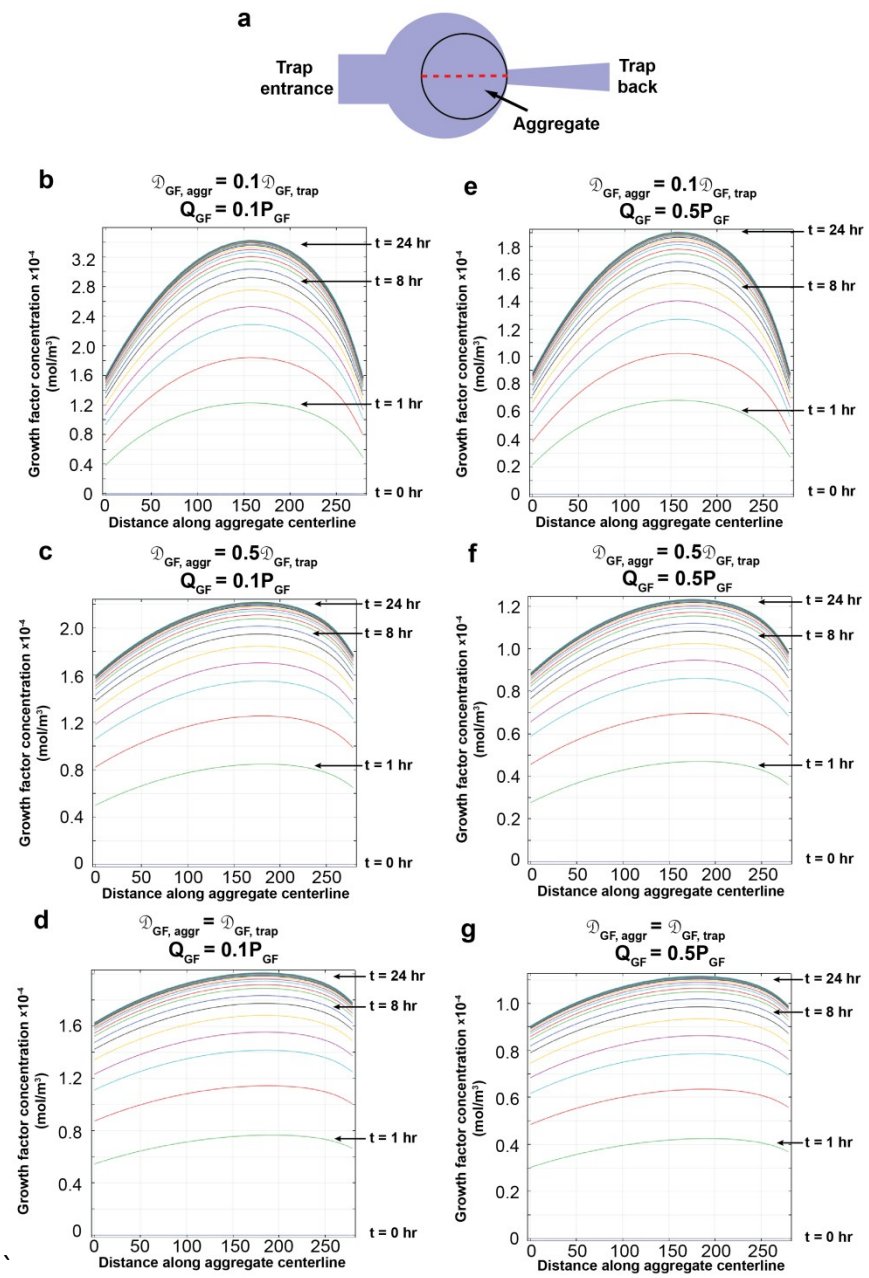

Supplemental Figure 11. Modeling production and consumption of a cell-secreted growth factor. a) Geometry modeled. b-g) Concentration of the growth factor along the horizontal centerline of the aggregate (as depicted in red in a) for 0-24 hours for three different values of the diffusion coefficient in the aggregate ($D_{GF,aggr}$) three different consumption rates (Q_{GF}). (P_{GF}) indicates secretion rate. Each line represents a time point from 0 to 24 hours, with a step of 1 hour. Time increases vertically.

References:

1. McMurtrey, R. J. Analytic Models of Oxygen and Nutrient Diffusion, Metabolism Dynamics, and Architecture Optimization in Three-Dimensional Tissue Constructs with Applications and Insights in Cerebral Organoids. Tissue engineering. Part C, Methods 22, 221-249, doi:10.1089/ten.TEC.2015.0375 (2016).
2. Griffith, L. G. & Swartz, M. A. Capturing complex 3D tissue physiology in vitro. Nature reviews. Molecular cell biology 7, 211-224, doi:10.1038/nrm1858 (2006).
3. Kinney, Melissa, “Biophysical and biochemical control of three-dimensional embryonic stem cell differentiation and morphogenesis” PhD diss., Georgia Institute of Technology, 2014, https://smartech.gatech.edu/handle/1853/53465.